0026-895X/04/6501-85–98$20.00
MOLECULAR PHARMACOLOGY
Copyright © 2004 The American Society for Pharmacology and Experimental Therapeutics
Mol Pharmacol 65:85–98, 2004

Vol. 65, No. 1
2786/1120152
Printed in U.S.A.

Mechanism of HIV-1 Integrase Inhibition by Styrylquinoline Derivatives in Vitro

Eric Deprez, Sophie Barbe, Macieij Kolaski,[1] Hervé Leh, Fatima Zouhiri, Christian Auclair, Jean-Claude Brochon, Marc Le Bret, and Jean-François Mouscadet

Centre National de la Recherche Scientifique Unité Mixte Recherche 8113, Laboratoire de Biotechnologies et Pharmacologie génétique Appliquée, Ecole Normale Supérieure de Cachan, Cachan, France (E.D., S.B., M.K., C.A., J.-C.B., M.L.B., J.-F.M.); and Bioalliance Pharma, Paris, France (H.L., F.Z.)

Received July 3, 2003; accepted October 10, 2003

This article is available online at http://molpharm.aspetjournals.org

ABSTRACT

Styrylquinoline derivatives (SQ) efficiently inhibit the 3′-processing activity of integrase (IN) with IC_{50} values of between 0.5 and 5 μM. We studied the mechanism of action of these compounds in vitro. First, we used steady-state fluorescence anisotropy to assay the effects of the SQ derivatives on the formation of IN-viral DNA complexes independently of the catalytic process. The IC_{50} values obtained in activity and DNA-binding tests were similar, suggesting that the inhibition of 3′-processing can be fully explained by the prevention of IN-DNA recognition. SQ compounds act in a competitive manner, with K_i values of between 400 and 900 nM. In contrast, SQs did not inhibit 3′-processing when IN-DNA complexes were preassembled. Computational docking followed or not by molecular dynamics using the catalytic core of HIV-1 IN suggested a competitive inhibition mechanism, which is consistent with our previous data obtained with the corresponding Rous sarcoma virus domain. Second, we used preassembled IN-preprocessed DNA complexes to assay the potency of SQs against the strand transfer reaction, independently of 3′-processing. Inhibition occurred even if the efficiency was decreased by about 5- to 10-fold. Our results suggest that two inhibitor-binding modes exist: the first one prevents the binding of the viral DNA and then the two subsequent reactions (i.e., 3′-processing and strand transfer), whereas the second one prevents the binding of target DNA, thus inhibiting strand transfer. SQ derivatives have a higher affinity for the first site, in contrast to that observed for the diketo acids, which preferentially bind to the second one.

Integration of the HIV-1 DNA into the host genome ensures stable maintenance of the viral genome and perpetuation of the virus in the host organism. Therefore, this reaction, catalyzed by integrase (IN), is a key process in the life cycle of the virus. Inhibitors of therapeutic interest for AIDS exist. Inhibitors that act early in the replication cycle target reverse transcriptase and those that act later target protease. The high mutation rate of HIV means that drug resistance is emerging, making it necessary to develop new drugs with different targets (combined therapies). Thus, it is essential to find drugs that target alternative steps of the HIV-1 replication cycle. IN, the third enzyme of the Pol precursor protein, is then an attractive target for novel drugs because of its central role in the HIV-1 life cycle.

IN is a 32-kDa protein (288 amino acids) that consists of three functional domains. The central domain (or core domain, residues 50–210) contains the catalytic triad (DDE) that is essential for enzymatic activity. This domain is flanked by the N-terminal domain (which has a role in the assembly of an active multimeric form of the enzyme) and the C-terminal domain (which has a role in the nonspecific DNA-binding activity). These three domains, protein oligomerization, the integrity of the catalytic triad, and a cationic cofactor such as magnesium are all necessary for IN activity (for review, see Craigie, 2001). The integration process requires two distinct catalytic steps. During the first step, termed *3′-processing*, IN specifically removes two nucleotides from each end of the linear viral DNA. The second step, called *strand transfer*, occurs after the translocation of the viral DNA into the nucleus. During this step, IN transfers both extremities of the viral DNA into the target DNA by a one-step transesterification reaction, resulting in full-site integration. Obviously, DNA-IN complex assembly is a prerequi-

This work was supported in part by the French national agency of research against AIDS (ANRS) and Ensemble Contre le Sida. J.-F.M., J.-C.B. and M.L.B. are funded by the Centre National de la Recherche Scientifique.

[1] Present address: Department of Theoretical Chemistry, Institute of Chemistry, Szkolna 9, 40-006 Katowice, Poland.

ABBREVIATIONS: IN, integrase; SQ, styrylquinoline; DTT, dithiothreitol; LTR, long-terminal repeat; DKA, diketo acids; MD, molecular dynamic(s); L-708,906, 4-(3,5-bis-benzyloxy-phenyl)-2,4-dioxo-butyric acid; 5-CITEP, 1-(5-chloroindo-3-yl)-3-hydroxy-3-(2H-tetrazol-5-yl)-propenone; EDC, 1-ethyl-3-(3-dimethylaminopropyl)carbodiimide.

site for the subsequent catalysis. In vitro, another reaction named disintegration can be observed when branched oligonucleotide substrates are used. In first approximation, this reaction represents the reversal of the half-site integration process (Chow et al., 1992). Interestingly, the central domain alone is capable of performing this reaction.

Many IN inhibitors have been characterized in vitro, but the biological activities of these drugs are generally poor, and little information concerning the mechanism of action is available in most cases (for review, see Pommier et al., 2000). It must be noted that most putative IN inhibitors were identified in vitro against Mn^{2+}- instead of Mg^{2+}-dependent IN activity. Because IN activity in the physiological context requires Mg^{2+} as the cationic cofactor, compounds that block the Mn^{2+}-dependent activity in vitro are less likely to possess antiviral activity. Active inhibitors can be divided into two groups: those that inhibit the 3′-processing reaction (most of the compounds) and those that preferentially inhibit the strand transfer reaction. The well known diketo acids (DKAs) and their more recent derivatives (Hazuda et al., 2000; Zhuang et al., 2003) belong to the second group and have good ex vivo activities against HIV replication, probably because of their ability to inhibit preassembled complexes. A recent study by Pommier and collaborators on a bifunctional DKA showed that the subdivision of IN inhibitors into two distinct groups is not so clear (Marchand et al., 2002). Our study on styrylquinoline (SQ) compounds leads to a similar conclusion.

SQ compounds (Fig. 1) described previously (Mekouar et al., 1998) act on the 3′-processing reaction in vitro, with IC_{50} values of between 500 nM and 5 μM. Several of them are efficient ex vivo with IC_{50} values in the micromolar range. We demonstrated that the 7-COOH and the 8-OH groups are essential for the inhibition activity (Zouhiri et al., 2000). Nevertheless, the mechanism of action of SQs remains unknown. Do these drugs act at the catalytic level or do they prevent substrate DNA-binding? Such molecular insights about the mechanism of action have been slow to emerge at least in part because of the experimental difficulties to separate the DNA-binding step from the subsequent catalysis reactions. Using a fluorescence-based DNA-binding assay, we show here that SQs prevent recognition of DNA by IN.

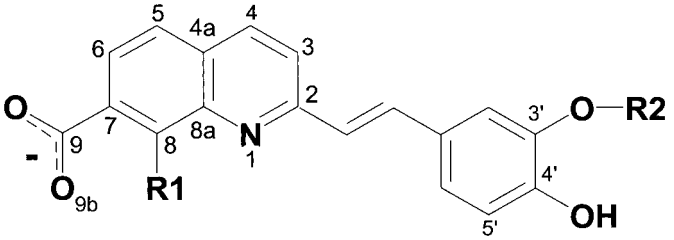

Compound	R1	R2	IC50 (3'-processing)
KHD161	OH	H	1.2 μM
FZ55	OH	CH_3	2.5 μM
FZ117	H	CH_3	>100 μM

Fig. 1. Chemical structures and IC_{50} of styrylquinoline compounds.

The IC_{50} values are in good agreement with those obtained in classic inhibition studies of the 3′-processing activity. This competitive mechanism is supported by molecular docking of these drugs on the HIV-1 catalytic core. In contrast, no inhibition was observed when the IN-DNA substrate complex was formed before adding the drug. Nevertheless, SQs were found to be potent inhibitors of the strand transfer reaction performed by the preassembled, preprocessed DNA-IN complexes, suggesting that two SQ-binding modes exist. We used computational docking data to propose several possible SQ-binding sites to take into account experimental results.

Materials and Methods

SQ Compounds and Oligonucleotides. KHD161, FZ55 and FZ117 (Fig. 1) were synthesized as described previously (Zouhiri et al., 2000; Polanski et al., 2002). Oligonucleotides U5B, 5′-GTGTGGAAAATCTCTAGCAGT-3′; U5B-2, 5′-GTGTGGAAAATCTCTAGCA-3′; U5A, 5′-ACTGCTAGAGATTTTCCACAC-3′; U5B-F, 5′-**F**-GTGTGGAAAATCTCTAGCAGT-3′ (where **F** designates the fluorescein probe); LDS32Bp, 5′-*p*-ACCCTTTTAGTCAGTGTGGAAAATCTCTAGCA-3′; LDS31A, 5′-ACTGCTAGAGATTTTCCACACTGACTAAAAG-3′; T1A, 5′-AGTGAATTAGCCCTTGGTCA-biotin; and T1B, 5′-TGACCAAGGGCTAATTCACT-biotin were purchased from Eurogentec (Seraing, Belgium) and further purified on an 18% denaturing acrylamide/urea gel. The phosphate residue present at the 5′-extremity of LDS32Bp was used to attach the target oligonucleotide covalently to the amino-Covalink surface (Merck Eurolab, Fontenay-sous-Bois, France). Terminal bases removed by IN during the 3′-processing reaction are underlined.

Fluorescence Properties of SQ in the Presence of IN. Excitation and emission spectra of FZ55 were performed on a Cary-Eclipse fluorescence spectrophotometer (Varian, Palo Alto, CA) thermostated at 25°C. Spectral study of FZ55 with varying concentrations of IN was performed in a Tris buffer (20 mM, pH 7.2) containing 100 mM NaCl. Quenching of the FZ55 steady-state fluorescence by Mg^{2+} was analyzed by a Stern-Volmer plot (i.e., by plotting $F_0/F-1$ as a function of Mg^{2+} concentration, where F_0 and F represent the fluorescence intensities in the absence and in the presence of quencher, respectively). Time-resolved fluorescence experiments for lifetime determination of FZ55 in the absence or in the presence of Mg^{2+} (60 mM) were performed by single-photon counting as described previously (Deprez et al., 2000, 2001) in the same conditions used as for the steady-state study (25°C, 30 μM FZ55). Excitation and emission wavelengths were 320 and 538 nm ($\Delta\lambda$ = 15 nm), respectively, with the emission polarizer oriented at the magic angle (54.7°). No photobleaching was observed during the acquisition and photons were collected until the total count reached 12 to 15 million.

Purification of IN and Standard Activity Assays. IN was expressed and purified as described previously (Leh et al., 2000). For activity assays, 100 pmol of either U5B (3′-processing substrate) or U5B-2 (strand transfer substrate) were radiolabeled using T4 polynucleotide kinase and 50 μCi of [γ-^{32}P]ATP (3000 Ci/mmol). The T4 kinase was then heat-inactivated, and unincorporated nucleotides were removed by filtration through a Sephadex G-25 column (Amersham Biosciences AB, Uppsala, Sweden). NaCl was added to a final concentration of 100 mM and the complementary unlabeled strand U5A was added. The mixture was incubated at 90°C for 3 min and allowed to anneal by slowly cooling to room temperature. The 3′-processing and strand transfer reactions were performed using 1.5 nM U5A/U5B and 10 nM U5A/U5B-2 double-stranded oligonucleotide substrates, respectively, in a buffer containing 20 mM HEPES, pH 6.8, 7.5 mM $MgCl_2$, and 2 mM DTT in the presence of various concentrations of IN. The reaction mixture was incubated for 1 h at 37°C and stopped by phenol-chloroform extraction. DNA products were precipitated with ethanol, dissolved in a loading buffer contain-

ing 7 M urea and 10 mM EDTA and subjected to electrophoresis on an 18% denaturing acrylamide/urea gel. Gels were dried and the reaction products were visualized using a STORM PhosphorImager (Amersham Biosciences).

Immobilized IN-DNA Complex Activity Assay: Microtiter Plate Assay. The strand transfer activity of the preformed complex was assayed in a 96-well microtiter plate coated with the U5–2 substrate as described previously (Hazuda et al., 1994). Briefly, the DNA substrate was coupled to the Covalink NH plates as follows: 75 μl of 100 nM double-stranded oligonucleotides LSD32Bp/LSD31A were placed into each well of the Covalink NH plates. Twenty-five microliters of 0.2 M EDC dissolved in 10 mM 1-MeIm7 was then added, and plates were incubated at 50°C for 5 h. Free oligonucleotides were removed and unreacted amino groups were deactivated by adding 10 mM citraconic anhydride. After 30 min at 50°C, the wells were finally washed with 5× standard saline citrate and 0.25% SDS. IN (100 nM) was then incubated with the substrate for 20 min at 25°C. The supernatant was discarded and 130 nM of the biotinylated target oligonucleotides were added in a final volume of 40 μl (the target double-stranded DNA was obtained by annealing the two complementary strands T1A and T1B in a 20 mM Tris-HCl buffer, pH 7.2, containing 0.1 M NaCl). The reaction was allowed to proceed for 1 h at 37°C and stopped by the addition of 0.1 M NaCl and 50 mM EDTA. The plates were washed twice for 5 min in washing buffer (0.05% Tween 20 and 10 μg/ml bovine serum albumin in phosphate-buffered saline). Extravidine phosphatase (Sigma; 100 μl of a 1/10,000 dilution in washing buffer) was added and incubated for 15 min at room temperature. The plates were washed twice in a 0.1 M Tris buffer pH 9 containing Tween + bovine serum albumin, 0.1 M NaCl, 50 mM $MgCl_2$. Finally, 100 μl of AP substrate were added and the reaction was allowed to proceed for 1 h at 37°C. Luminescent signal was recorded on a microtiter plate photometer (Dynatech Labs, Chantilly, VA).

DNA-Integrase Binding Assay. The interaction between IN and the fluorescein-labeled oligonucleotide was detected by fluorescence anisotropy. The double-stranded oligonucleotide was obtained by mixing equimolar amounts of complementary strands U5B-F and U5A in a 20 mM Tris-HCl buffer, pH 7.2, containing 100 mM NaCl. The mixture was heated to 85°C for 5 min and allowed to anneal by slowly cooling to room temperature. The steady-state anisotropy measurements were recorded on a Beacon 2000 instrument (PanVera, Madison, USA). To determine the apparent K_d value, fluorescein-labeled DNA (1 nM) was incubated with increasing concentrations of IN in a 20 mM Tris buffer, pH 7.2, containing 1 mM DTT, 25 mM NaCl, and 5 mM $MgCl_2$ for 20 min at 25 or 37°C. Steady-state anisotropy was then recorded in a cell thermostated at 25 or 37°C. The fractional saturation Y was calculated as $(A - Af)/(Ab - Af)$, where Ab and Af represent the bound and free DNA anisotropy, respectively, because no significant concomitant change in the fluorescence intensity was observed. For cooperative binding, the Hill number, n, was calculated from the plot LOG $(Y/1 - Y)$ = F(LOG(IN)). The concentration of IN required to titrate the DNA to half saturation was IN_{50} or apparent K_d and was equal to $K_d^{1/n}$.

IC^{50} values were determined by measuring Y in the presence of increasing concentrations of drugs. IN was preincubated with drugs for 10 min at 25 or 37°C in a 20 mM Tris buffer, pH 7.2, containing 25 mM NaCl, 5 mM $MgCl_2$, and 1 mM DTT. Complexes with DNA were then allowed to form at 25 or 37°C after the addition of double-stranded fluorescein-labeled oligonucleotides. The midpoint or IC_{50} of the inhibition curve represents the total drug concentration giving 50% inhibition ($Y = 0.5$) and was used to estimate the K_i value. K_i was determined by use of the following equations, which are based on a competitive inhibition model. At equilibrium,

$$IN + DNA \leftrightarrow IN\text{-}DNA \text{ and } IN + i \leftrightarrow IN\text{-}i$$

with

$$K_d = \frac{[IN]^n \cdot [DNA]}{[IN\text{-}DNA]} \quad (1)$$

and

$$K_i = \frac{[IN] \cdot [i]}{[IN\text{-}i]} \quad (2)$$

where IN, DNA, and i are the concentrations of free integrase, DNA substrate, and inhibitor, respectively, $IN \cdot DNA$ and $IN \cdot i$ designate the complexes, and n is the average number of interacting sites.

The concentrations of total IN, DNA substrate, and inhibitor are calculated as follows,

$$[IN_T] = [IN] + n \cdot [IN\text{-}DNA] + [IN\text{-}i] \quad (3)$$

$$[i_T] = [i] + [IN\text{-}i] \quad (4)$$

$$[DNA_T] = [DNA] + [IN\text{-}DNA] \quad (5)$$

using eqs. 2 and 4,

$$\frac{1}{[IN]} = \frac{[i_T]}{K_i \cdot [IN\text{-}i]} - \frac{1}{K_i} \quad (6)$$

using eqs. 1 and 5,

$$\frac{1}{[IN]} = \left(\frac{1 - Y}{K_d \cdot Y}\right)^{\frac{1}{n}} \quad \text{with} \quad Y = \frac{[IN\text{-}DNA]}{[DNA_T]} \quad (7)$$

Eqs. 6 and 7 yield:

$$\left(\frac{1}{K_d} \cdot \left(\frac{1}{Y} - 1\right)\right)^{\frac{1}{n}} = \frac{1}{K_i} \cdot \left(\frac{[i_T]}{[IN\text{-}i]} - 1\right) \quad (8)$$

Substitution of eq. 3, i.e.,

$$[IN - i] = [IN_T] - \left(\frac{K_d - Y}{I - Y}\right)^{\frac{1}{n}} - n \cdot Y \cdot [DNA_T]$$

into eq. 8 yields:

$$\left(\frac{1}{K_d} \cdot \left(\frac{1}{Y} - 1\right)\right)^{\frac{1}{n}} = \frac{1}{K_i} \cdot \left(\frac{[i_T]}{[IN_T] - \left(\frac{K_d \cdot Y}{1 - Y}\right)^{\frac{1}{n}} - n \cdot Y \cdot [DNA_T]} - 1\right) \quad (9)$$

Eq. 9 is equivalent to:

$$[i_T] = \left(K_i \cdot \left(\frac{1}{K_d} \cdot \left(\frac{1}{Y} - 1\right)\right)^{\frac{1}{n}} + 1\right) \cdot \left([IN_T] - \left(\frac{K_d \cdot Y}{1 - Y}\right)^{\frac{1}{n}} - n \cdot Y \cdot [DNA_T]\right) \quad (10)$$

Assuming saturation conditions in the absence of inhibitor (i.e., $Y = 1$), eq. (10) can be simplified at the IC_{50} value where $Y = 0.5$.

$$K_i = \left(\frac{IC_{50}}{[IN_T] - K_d^{\frac{1}{n}} - \frac{1}{2} \cdot n \cdot [DNA_T]} - 1\right) \cdot K_d^{\frac{1}{n}} \quad (11)$$

The independent measurements of IN_{50} or $K_d^{1/n}$ and IC_{50} allowed the calculation of K_i using eq. 11.

Computer Studies and Protein Conformations

The computer studies used two models for the molecular target of the drug. The first one, hereafter called a, was the catalytic core

(residues 50–212) of the HIV-1 IN containing the single mutation F185H with an Mg^{2+} cation in its active site. The conformation was the frame obtained after 3.4275 ns of production of a 4-ns molecular dynamics simulation (Laboulais et al., 2001). This frame was selected because the Glu152 carboxylic group pointed to the other two triad members Asp64 and Asp116 in a geometry that is compatible with the catalysis. The flexible loop (139–151) is not as stacked onto the catalytic core as found in the structure 1QS4 (Goldgur et al., 1999) but closely resembles the structures described by Maignan et al. (1998). The model was then stripped of the chloride anion. Two submodels were derived. In submodel a_0, no water molecules were retained, whereas in submodel a_4, the four water molecules coordinated to Mg^{2+} were explicitly retained. The other model, hereafter called b, was the 55–209 fragment of the HIV-1 IN catalytic core containing the mutations W131E, A133G, and F185K. The conformation was taken from the coordinates of monomer A in the crystal structure 1QS4 (Goldgur et al., 1999). Missing residues were forced to have the same backbone dihedrals as in the crystal structure 1BIS (Goldgur et al., 1998). The model was then stripped of all water molecules, giving the submodel b_0; in submodel b_4, the four water molecules coordinated to Mg^{2+} were explicitly retained.

Docking

The target (a_0, a_4, b_0, or b_4) was digitized on an orthorhombic grid containing $256 \times 256 \times 256$ meshes of size $0.305 \times 0.305 \times 0.297$ Å^3. The structure of the drug KHD161 was optimized as described previously (Ouali et al., 2000) and the tautomeric form with the 7-COO^- and 8-OH groups was used. The drug was rotated by 12° increments and for each of these 12,660 orientations, the translations giving the best overlap were stored when the electrostatic drug-target interaction energy was favorable. As described previously (Ouali et al., 2000), the best 1000 overlapping complexes and the most favorable 200 complexes for the pure electrostatic interaction were minimized, with both drug and target being optimized. During the minimization, the aqueous medium was implicitly represented through a sigmoidal distance-dependent dielectric constant (Lavery et al., 1986). The 1200 complexes were sorted according to the drug-protein interaction energy, which is the sum of the van der Waals and Coulomb contributions.

Clustering

The 100 most favorable complexes were stored and the 100×100 root-mean-squared Euclidean distances of the drug atom coordinates were further transformed into a dendrogram representing the hierarchy of categories of clusters. The hierarchical and agglomerative processes work as follows. Starting from a set of $n = 100$ clusters, one per drug position and orientation, a sequence of clusterings was grown until all n patterns were in a single cluster. At each step, the two closest clusters were reunited. The distance separating the remaining clusters from the newly created cluster was the weighted average of the distances to the members of the new cluster (Laboulais et al., 2002). The results of the clustering analysis are shown in Fig. 3 and Table 2.

Molecular Dynamics

The catalytic core-drug complexes obtained using an implicit solvent representation at the end of the docking (conformation a_0) had the net coulombic charge of one proton. A chloride anion was then added and the whole system was embedded in a $52.3 \times 52.3 \times 52.3$-Å^3 box filled with 3638 transferable intermolecular potential (TIP3P) water molecules. The SANDER module of AMBER (P. Kollman, University of California, San Francisco) was used to simulate the dynamics. Long-range coulombic interactions were calculated using the particle-mesh technique for Ewald sums (Ewald, 1921) with a cut-off of 10 Å and a $50 \times 50 \times 50$-point grid. No correction was applied for the neglected long-range van der Waals interactions because they were expected to be small. Covalent bonds containing a proton were constrained to their equilibrium length by use of the SHAKE algorithm (Ryckaert et al., 1977). The elementary integration time step was 2 fs. Before dynamics could be reliably produced, the system was prepared by two heating steps. In the first step, only the water molecules were allowed to move and the temperature was increased from 25 to 300 K in 25-K steps during 14.6 ps. At the end of this first step, water molecules were cooled to 10 K. In a second step, the temperature of the whole system was increased from 10 to 300 K over 18 ps. The velocities were then equilibrated for 13 ps at 300 K, before starting dynamics production. Frames were then recorded at 0.1-ps intervals. The total duration of the molecular dynamics simulations was 2 ns.

Results

Docking of KHD161 to the Catalytic Core Domain of IN. To get some clue about the location of the binding site on the HIV-1 IN catalytic core, we carried out a number of docking simulations with the KHD161 compound (Fig. 1). The first step of the procedure was based on rigid docking and the second on an MD approach. After rigid docking and minimization using an implicit representation of the solvent (model a_0), the best target-drug complexes were selected according to their interaction energies (coulombic and van der Waals). For all the best 17 complexes, KHD161 was found near the essential catalytic cofactor Mg^{2+}. In all cases, at least one oxygen atom of the drug was within 3 Å of the Mg^{2+} ion, and the drug-target interaction energies ranged from −115 to −87 kcal/mol. The best two complexes (d1 and d2) were used as starting conformations for MD. Some features of the dynamics d1 and d2 are summarized in Table 1.

In d1, Mg^{2+} bound to O8 and O9b of the quinolic ring. The catechol ring was stacked over the phenol group of Tyr143. Figure 2 shows how some distances changed over time in the

TABLE 1
Parameters of HIV-1 catalytic core-KHD161 complexes according to computational docking and molecular dynamics studies

	Complex	
	d1	d2
Interaction energy (kcal/mol) (implicit solvent representation) before MD	−114.97	−97.4
Average energy in the presence of 3638 explicit water molecules (kcal/mol). Fluctuations are indicated in parentheses		
From 0 to 1 ns	−31,494.4 (353.8)	−31,479.8 (317.9)
From 1 to 2 ns	−31,513.5 (45.2)	−31,507.1 (46.8)
Contacting residues after docking and minimization and before MD	Thr66, Asp116, Phe139, Gly140, Ile141, Pro142, Tyr143	Asp64, Thr66, His67, Leu68, Asp69, Glu152, Lys159
Contacting residues after 2 ns of dynamic simulation	Asp64, Asp116, Tyr143, Gln148, Glu152	Asp64, Cys65, Thr66, Glu152, Asn155

subsequent MD. Time 0 is the beginning of the production phase (the preparation phase is not shown). Although some motion was observed, the drug remained in the same position as at the beginning of the dynamics. For instance, the average distances separating the oxygen atoms O9b (Fig. 2a) and O8 (not shown) from the Asp64 of the catalytic triad Asp64-Asp116-Glu152 were the same from the start of the docking step until the end of the dynamics simulation. Some changes occurred only during the preparation phase. Residues Asp116 and Glu152, which were 4 and 7 Å from the drug oxygen atoms O8 and O9b, moved nearer to these atoms during the preparation phase, but remained at the same distance throughout the production phase (Fig. 2, b and c). Other distances fluctuated much more, such as those separating the drug from Tyr143 and Gln148 (Fig. 2, d and e). During the simulation, water molecule 2631 came into close contact with Gln148 and the drug several times, but only transitorily. At the end of the simulation (2 ns), this water molecule joined Gln148 to the quinoline proton H4, Gln148 being close to the quinoline proton H5. The pattern shown in Fig. 2f suggests that the water molecule is not stable in the active site.

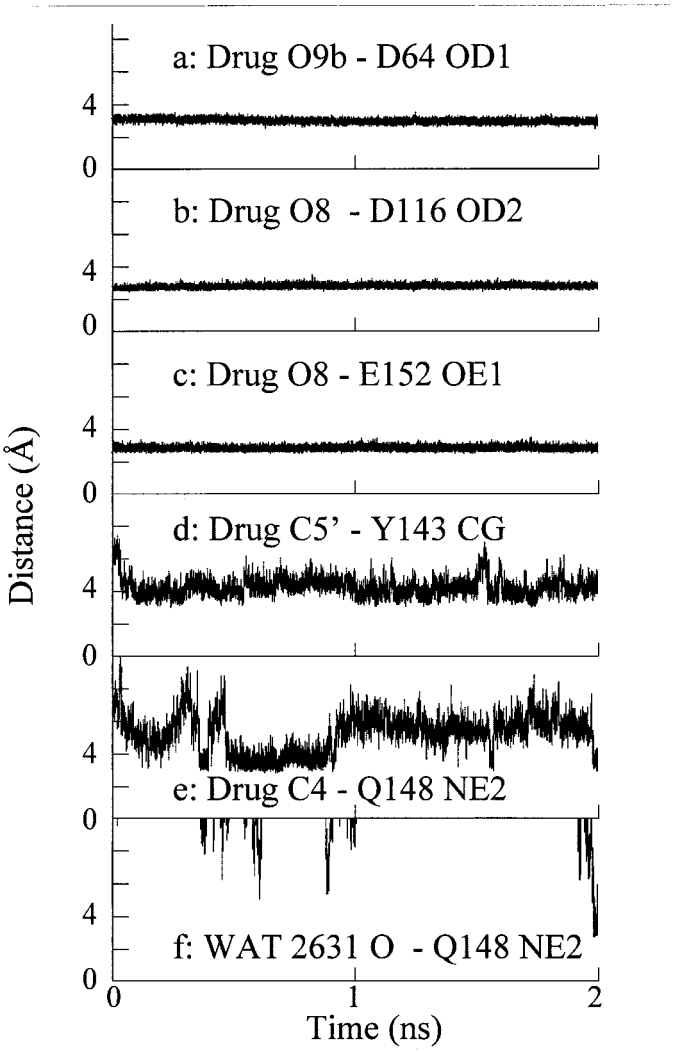

Fig. 2. Changes in selected distances (Ångstroms) with time (nanoseconds) in the d1 dynamics. The time scale started at the beginning of the production phase. a, drug O9b-Asp64 OD1; b, drug O8-Asp116 OD2; c, drug O8-Glu152 OE1; d, drug C5′-Tyr143 CG; e, drug C4-Gln148 NE2; f, water 2631 O-Gln148 NE2.

The conformation d2 was less favorable. In this case, the drug bound to Mg^{2+} through the hydroxyl groups of the catechol ring. At the end of the MD, the catechol ring remained near Mg^{2+}, but the quinoline ring protruded from the protein structure in the solvent (not shown). This result was not observed with d1. Our simulation results indicate that d1 is characterized by more favorable interaction energy after the docking and is also more stable in the active site during the dynamics. During both dynamics d1 and d2, no water molecule formed a steady interaction with both the drug and the protein. This is in contrast to the 1-(5-chloroindol-3-yl)-3-hydroxy-3-(2H-tetrazol-5-yl)-propenone complex (5-CITEP) (Ni et al., 2001). This explains why the interaction energies calculated using an implicit representation of the solvent and the average energies calculated over 1 ns were of the same order. Only the energy fluctuation was much lower during the second nanosecond than during the first (see Table 1). For both d1 and d2, some key residues found to form contacts with KHD161, for instance Tyr143, Gln148, and Lys159 (see Table 1), have previously been described to form contacts with DNA (Jenkins et al., 1997; Esposito and Craigie, 1998), suggesting that the location of SQ within the active site is incompatible with DNA-binding. The results were not significantly different when b_0 was used as a target (structure 1QS4) in the docking and minimization processes instead of a_0.

In the simulations described above (model a_0 or b_0), the protein was completely stripped of all its water molecules, allowing the drug to form direct contacts with Mg^{2+}. This overestimates the electrostatic interaction. It is more likely that some water molecules are sandwiched between the drug and the cation. Additional docking simulations were then carried out, with four water molecules surrounding Mg^{2+}. The introduction of four explicit water molecules into the models (models a_4 and b_4) had the following general consequences compared with simulations using a_0 and b_0 (note that no major difference was observed between a_4 and b_4, as was the case for a_0/b_0): 1) Because of the increase in the shortest distance separating the drug from Mg^{2+} (caused by the presence of water), drug-protein interaction energies were less favorable. 2) The hierarchy of interaction energies for the different binding sites was not similar between the a_4/b_4 models and the a_0/b_0 models. For instance, a binding localization came up in the 3rd rank in model a_4 compared with in the 18th rank in model a_0. 3) Although some differences were observed when a_4/b_4 were compared with a_0/b_0, the drug was still in contact with the hydrated Mg^{2+} in the most favorable localization even if the presence of water molecules decreased the role of Mg^{2+} in the stabilization of the drug-protein complex. 4) Energy in the a_4 or b_4 model was not as widespread as in the a_0 or b_0 model.

Because no clear differences were observed between a_4 and b_4, the best 100 complexes were pooled and classified by clustering analysis (see *Materials and Methods*) without any energy considerations to identify different sites. Three main sites were identified. Stereoviews of representative complexes for each cluster are shown in Fig. 3, and Table 2 summarizes the main features of the various clusters (e.g., population, energy statistics, and contacting residues). The contacting residues of cluster 1 (Fig. 3A) overlap the catalytic

triad. Note that d1 and d2 as obtained after rigid docking and MD belong to this cluster. Cluster 2 is actually made of a succession of overlapping sites and is spread over a large region of the protein surface (Fig. 3B) whereas a small number of conformations form the cluster 3 (Fig. 3C). The influence of Mg^{2+} is only significant in cluster 1 and explains why the average interaction energy was better for this cluster. As expected, the negative drug bound to lysine-rich regions. The lysine residues can be very roughly clustered into two groups: group 1 contains Lys156, Lys159, Lys160, Lys186, and Lys188, whereas group 2 contains Lys111 and Lys136. From this point of view, clusters 1 and 2 belong to group 1 whereas cluster 3 belongs to group 2. Residues Lys156 and Lys159 in cluster 1 and residue Lys136 in cluster 3 have been previously found to be involved in DNA binding (Mazumder et al., 1996; Jenkins et al., 1997). Besides the lysine residues, Gln148 and Tyr143, contained in clusters 1 and 3, respectively, are also key residues for DNA binding, as shown by photo–cross-linking experiments (Esposito and Craigie, 1998). Another residue in cluster 1, Ser119, is important for DNA binding because mutation of this residue affects target site selection (Harper et al., 2001). No residues from cluster 2 are known to be essential for DNA binding.

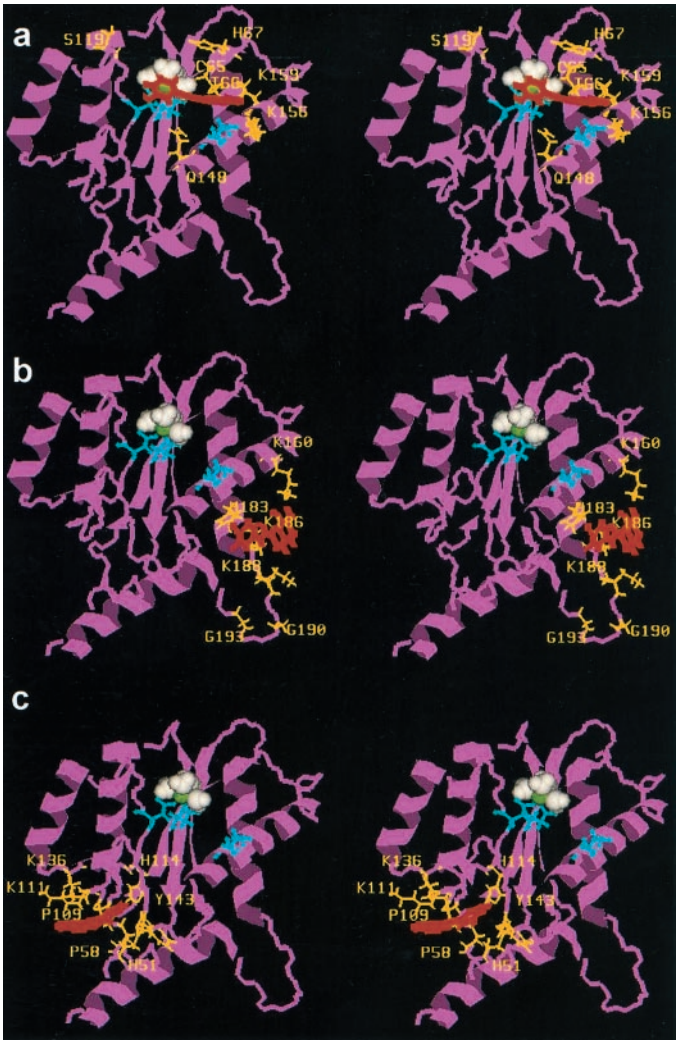

Fig. 3. Stereoview of one SQ-IN complex conformation belonging to each cluster. The different clusters were obtained as described under *Materials and Methods*. Only a typical conformation is shown among various orientations which were clustered together. a, cluster 1; b, cluster 2; c, cluster 3. The detailed clustering analysis is shown in Table 2. Magenta, protein; green, Mg^{2+}; white, water; red, drug. The catalytic triad (Asp64-Asp116-Glu152), is shown in cyan (sticks and balls), and contacting residues are in yellow.

Influence of IN on the Fluorescence Emission Spectrum of FZ55. A fluorescence study of SQ in the absence or in the presence of IN was carried out to get experimental support of the existence of IN-SQ complexes. As found previously (Ouali et al., 2000; Zouhiri et al., 2000) and confirmed in this study (see below), the in vitro inhibition properties of SQ derivatives originate in the simultaneous presence of both C7-COOH and C8-OH groups in the quinoline subunit and are less sensitive to modifications at the C3′ or C4′ positions. Accordingly, KHD161 and FZ55 are characterized by very similar inhibition properties. For stability reasons (Burdujan, 2002), FZ55 was preferred over KHD161 in the following spectral study. Excitation and emission spectra of FZ55 are shown in Fig. 4a. Excitation maximum is centered at 330 nm, whereas emission maximum is centered at 538 nm. During our study, we found that Mg^{2+} (the essential cofactor for IN activity) acts as a quencher of fluorescence for FZ55, suggesting that SQs could not be a competitive inhibitor but simply a chelation agent. In other words, Mg^{2+} could be displaced from the active site in the presence of SQs, and the inhibition process could then occur independently of the drug binding within the active site. We then performed Stern-Volmer analysis to quantify the quenching process (Fig. 4b). The Stern-Volmer plot was linear and similar slopes were obtained at two different excitation wavelengths, 320 and 345 nm. Note that quenching can be caused by two distinct phenomena at the molecular level, dynamic or static, each leading to the overall decrease of fluorescence intensity and linear Stern-Volmer plot. Only in the case of static quenching does a stable complex exist that is nonfluorescent. In contrast, dynamic quenching is caused by a collisional process that occurs during the lifetime of the excited state. This means that the lifetime is not influenced in the case of static quenching, whereas it decreases in the case of collisional quenching. Because the two phenomena can be distin-

TABLE 2
Clustering of the best 100 complexes obtained after docking of KHD161 to the a_4 and b_4 IN catalytic core

Cluster	Population	Average Energy	Lowest Energy	Highest Energy	Contacting residues (<5 Å)	No of Lysine Groups
			kcal/mol			
1	19	−70.0	−92.8	−61.6	Asp64 Cys65 Thr66 His67 Asn92 Asp116 Asn117 Gly118 Ser119 Asn120 Gln148 Glu152 Asn155 Lys156 Lys159	1
2	42	−67.7	−77.1	−61.4	Glu157 Lys160 Ile161 Gln164 His183 Lys186 Lys188 Gly189 Gly190 Gly193 Tyr194 Ser195 Ala196 Arg199	1
3	7	−65.9	−70.9	−62.9	His51 Ser57 Pro58 Gly59 Ile60 Pro109 Lys111 Thr112 His114 Lys136 Pro142 Tyr143	2

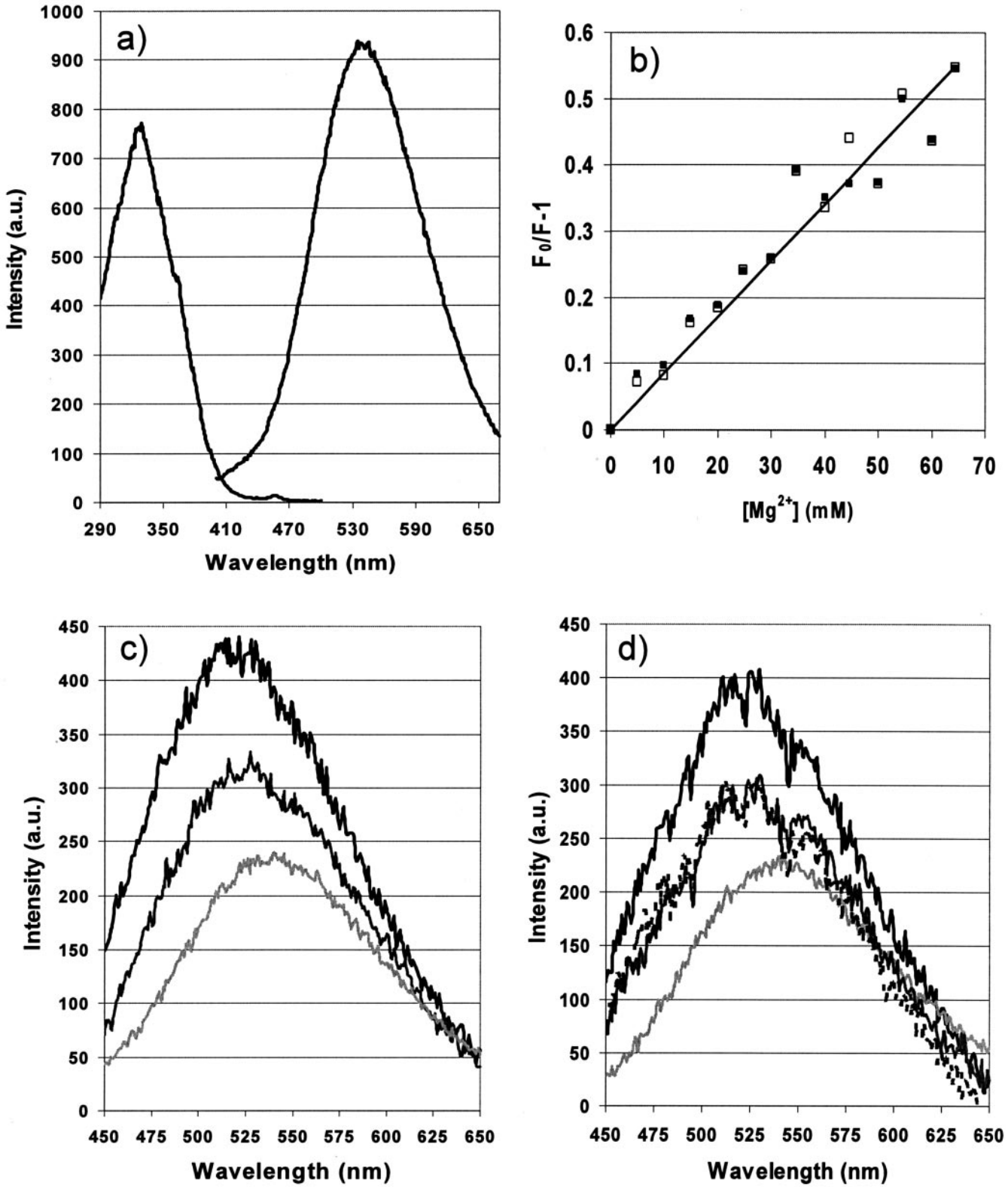

Fig. 4. Fluorescence properties of free and IN-bound FZ55. a, excitation and emission spectra of FZ55 (30 μM). Excitation (λ_{em} = 538 nm) and emission (λ_{exc} = 345 nm) spectra were obtained at 25°C. Emission and excitation slit widths were 5 nm. b, Stern-Volmer representation for the quenching of FZ55 by Mg^{2+}. F_0 and F are the intensities of emission fluorescence at 538 nm in the absence and in the presence of Mg^{2+}, respectively. FZ55 concentration, 30 μM. □, excitation at 320 nm. ■, excitation at 345 nm. c, influence of IN on the emission spectrum of FZ55 (λ_{exc} = 345 nm). Concentration of FZ55 was 3 μM in a Tris buffer (20 mM, pH 7.2) containing 100 mM NaCl and 5 mM Mg^{2+}. Light gray, no IN; dark gray, IN 0.9 μm; black, IN 3 μM. d, influence of Mg^{2+} on the emission spectrum of IN-bound FZ55 (λ_{exc} = 345 nm). Light gray, FZ55 3 μM without IN in the presence of 5 mM Mg^{2+}; dark gray, 3 μM FZ55 with 3 μM IN in the absence of 5 mM Mg^{2+}; black, 3 μM FZ55 with 3 μM IN in the presence of 5 mM Mg^{2+}; dashed line, 3 μM FZ55 with 3 μM IN in the presence of 1 mM EDTA. NaCl concentration was 100 mM.

guished by lifetime measurements, we then performed time-resolved fluorescence experiments in the absence or in the presence of 60 mM Mg^{2+} (λ_{exc} = 320 nm). The average lifetimes as well as lifetime distributions of FZ55 were unchanged in both conditions (τ_1 = 18 ± 2 ps (33%)/τ_2 = 70 ± 11 ps (5%)/τ_3 = 242 ± 4 ps (54%)/τ_4 = 490 ± 6 ps (8%)/$\tau_{average}$ = 175 ps) demonstrating that the Mg^{2+}-dependent quenching of FZ55 is static. The slope of the Stern-Volmer plot shown in Fig. 4b corresponds then to an association constant K_a = 8.6 M^{-1} (i.e., K_d = 120 mM). This value definitively ruled out the idea that IN inhibition by SQs, characterized by submicromolar or micromolar IC_{50} in the presence of 5 mM Mg^{2+}, could be simply caused by the chelation of Mg^{2+}. It is then unlikely that SQs inhibit IN by displacing the essential Mg^{2+} cofactor from the active site.

Next, we studied the influence of IN-binding on the fluorescent properties of FZ55. As shown in Fig. 4c, increasing concentrations of IN (entire protein) enhanced fluorescence intensity and blue-shifted the maximum of emission. This phenomenon is less pronounced in the absence of Mg^{2+} or in the presence of EDTA (Fig. 4d) indicating that first, FZ55 actually binds to IN and second, the stability of the complex is dependent on the presence of Mg^{2+}, in accordance with the docking results. Similar conclusions had been previously published in the case of the catalytic core (Burdujan, 2002). It is then very likely that the inhibition property of SQs is related to their capabilities to bind within the protein.

Inhibitory Effect Is Caused by the Ability to Impair DNA Binding. Even though we do not yet know how the IN active unit is organized, recent molecular docking of a dinucleotide onto the IN core domain has revealed two possible nucleic acid-binding sites on a single monomer (Perryman and McCammon, 2002). One of these sites encompasses a previously described nucleotide-binding site that involves three lysine residues of the catalytic core domain, Lys156, Lys159, and Lys160 (i.e., cluster 1 in our study) (Jenkins et al., 1997; Drake et al., 1998; Jing et al., 2000). These lysine residues are involved in the binding of viral DNA (i.e., donor DNA) (Jenkins et al., 1997). The second site is a putative binding site for the target or cell DNA (i.e., acceptor DNA). Our molecular docking study strongly suggested that the location of the SQ drug within the active site mainly disturbs the binding of viral DNA to the core domain of the IN. To address this hypothesis, we used steady-state fluorescence anisotropy to investigate the effects of SQs on the binding of IN to a short double-stranded substrate DNA (21-mer). One major difficulty encountered when studying of DNA binding properties of HIV-1 IN is the separation of the elementary DNA-binding process from the subsequent activity steps (i.e., 3′-processing and strand transfer). It is then a difficult task to separate the molecular and physicochemical effects on these different steps by only measuring the overall activity by classic enzymatic assays. Note that the enzymatic assays involving IN described in the literature do not correspond to Michaelis-Menten conditions, meaning that "k_{cat}" and "V_{max}" values should be interpreted with caution. Steady-state anisotropy measurements are based on the principle of depolarization of light by a fluorescent probe caused by the rotational diffusion that occurs between excitation and emission. The degree of depolarization is related to rotational motion and flexibility properties of the molecular edifice that contains an intrinsic or extrinsic fluorophore. Low anisotropy is associated with a small edifice and high local flexibility, whereas high anisotropy is associated with a large edifice and low local flexibility. To study the DNA-IN interaction, fluorescein was attached to the extremity of a double-stranded oligonucleotide (21-mer) that mimicked the U5 viral LTR terminus. Fluorescein was attached through a 6-carbon linker to the opposite end from the processing site to prevent steric conflicts between IN and the fluorophore [similar 3′-processing and integration activities were detected when labeled or unlabeled DNA was used as a substrate (data not shown)].

The fluorescein-labeled oligonucleotides, free in solution, were characterized by a low anisotropy value, 0.048 and 0.060 at 37 and 25°C, respectively. When IN bound to the oligonucleotide, the steady-state fluorescence anisotropy increased. The upper limits of anisotropy values were 0.232 and 0.240 at 37 and 25°C, respectively, yielding a maximum amplitude of about 0.180. This value of the steady-state anisotropy may be explained by a combination of two phenomena, the slower global tumbling of the IN-DNA complex and the more restricted local motion of fluorescein. As shown in Fig. 5, this value decreased when the interaction was tested in the presence of KHD161. Data analysis of the KHD161 curves (■, □) yielded IC_{50} values of 1.50 ± 0.13 μM and 0.98 ± 0.09 μM at 37 and 25°C, respectively. The IC_{50} for the DNA-binding step at 37°C is compatible with the value found in activity tests (3′-processing reaction) at the same temperature in the presence of similar IN and substrate concentrations (IC_{50} = 1.2 μM). In contrast, concentrations of up to 10 μM of the structurally related compound FZ117 had no significant inhibitory effect [(DNA-IN interactions were weakened only above 50 μM FZ117 (data not shown)]. Again, this result is in accordance with the activity tests, because FZ117 had no effect on IN activity. Because the experimental conditions used in the DNA-binding assays were similar to those used in enzymatic assays, the IC_{50} values obtained in both cases (1.2–1.5 μM) can be compared. Consequently,

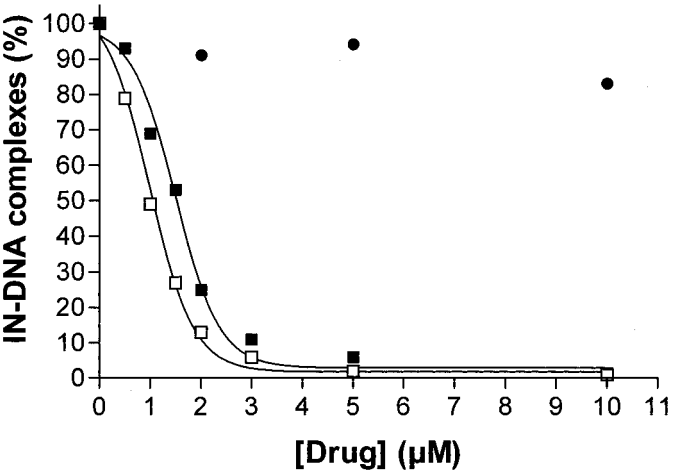

Fig. 5. Percentage of integrase-oligonucleotide complexes as a function of drug concentration. □, KHD161 at 25°C; ■, KHD161 at 37°C; ●, FZ117 at 25°C. Steady-state fluorescence anisotropies were measured at 25°C or 37°C as described in the text. The values were normalized based on the anisotropy amplitude values (complex minus free oligonucleotide). One hundred percent corresponds to an anisotropy amplitude of 0.180 (see text). IN concentration, 120 nM. The fit of the KHD161 curves using a sigmoidal shape gave IC_{50} values of 0.98 ± 0.09 μM and 1.50 ± 0.13 μM at 25 and 37°C, respectively.

DNA-binding inhibition probably accounts for the whole inhibition of enzyme activity, thus suggesting a competitive mechanism of action. Unlike when IN and KHD161 were preincubated before adding the DNA, the IN-DNA complex was not disrupted when IN and DNA were preincubated before adding the drug (data not shown).

To test the hypothesis of a competitive mode of action, we determined IC_{50} values at different protein concentrations, because the theory suggests that IC_{50} is related to IN concentration. Moreover, if this is case, K_i can be estimated from eq. 11. Note that the well known Cheng and Prusoff model (1973), which estimates K_i from IC_{50} values, is only valuable for classic enzymatic conditions (i.e., low enzyme concentration and excess substrate), when free substrate and inhibitor concentrations can be assumed to be equal to total concentrations. However, in the case of IN, the target of the inhibitor, the enzyme, is in excess compared with the DNA substrate. Thus, the Cheng-Prusoff relationship cannot be used because DNA and i (which represent concentrations of free DNA and inhibitor, respectively) are not equal to DNA_T and i_T, respectively. In contrast to the Cheng-Prusoff relationship, the Linden equation (Linden, 1982) represents the exact solution of K_i because it is not based simply on the assumption that free and total concentrations are approximately equal (this last assumption is often true for Michaelis-Menten conditions). Unfortunately, as is shown below, the Hill slope of the binding of IN to DNA is not equal to 1. In this case, the Linden equation is not valid. In our study, the estimation of K_i was based on the knowledge of the IC_{50} (which corresponds to the total inhibitor concentration, not free), the IN concentration used in the assay (again, the total concentration, not free), and the apparent K_d value or IN_{50}, using eq. 11.

The experiments were carried out with the SQ derivative FZ55, which has an inhibitory potency similar to that of KHD161 (the IC_{50} value of FZ55 for the 3′-processing reaction, 2.5 μM, is slightly higher than those obtained in same experimental conditions for KHD161). The saturation fraction, Y, as a function of total inhibitor concentration (i_T) is expected to be sigmoidal (see eq. 10). Accordingly, as shown in Fig. 6, $Y = f([i_T])$ was sigmoidal at four different IN concentrations (Fig. 6, a–d). IC_{50} values were then obtained from a sigmoidal model. To calculate the K_i values at two temperatures, 25 and 37°C, we first determined the apparent K_d values using the isotherm binding curves shown in Fig. 7. The results are summarized in Table 3. The apparent K_d value was rather constant in the 25 to 37°C temperature range, indicating that the enthalpic contribution to the IN-DNA complex formation is minor. Furthermore, the binding of DNA to IN exhibited a positive cooperativity at both temperatures (n = 1.81–1.88). As expected from eq. 11, the IC_{50} values were strongly dependent upon the experimental conditions (i.e., the IN concentration) (Table 4). Taking into account the various IN concentrations, the K_i values were rather similar for a given temperature (see the fourth column of Table 4), and average K_i increased slightly (from 620 to 890 nM) when the temperature was increased from 25°C to 37°C. This indicates that in contrast to the IN-DNA interaction, the binding of FZ55 to IN is not entropy-driven. The estimated enthalpy for the IN-FZ55 complex was about −5.6 kcal/mol, whereas the entropy was slightly negative. KHD161 is slightly better than FZ55. Taking into account the IC_{50} values found in Fig. 5, the calculated K_i for KHD161 at 25°C and 37°C are equal to about 400 and 680 nM, respectively. This agrees with the IC_{50} values found in activity tests. Note that K_i values can be calculated using eq. 11 only if fractional saturation is near or equal to 1 in the absence of inhibitor. This can be considered the case given the last column of Table 4.

Only a model using n different sites was able to fit the binding isotherm data. The Hill number, n, was found to be equal to approximately 1.9 by the binding isotherms shown

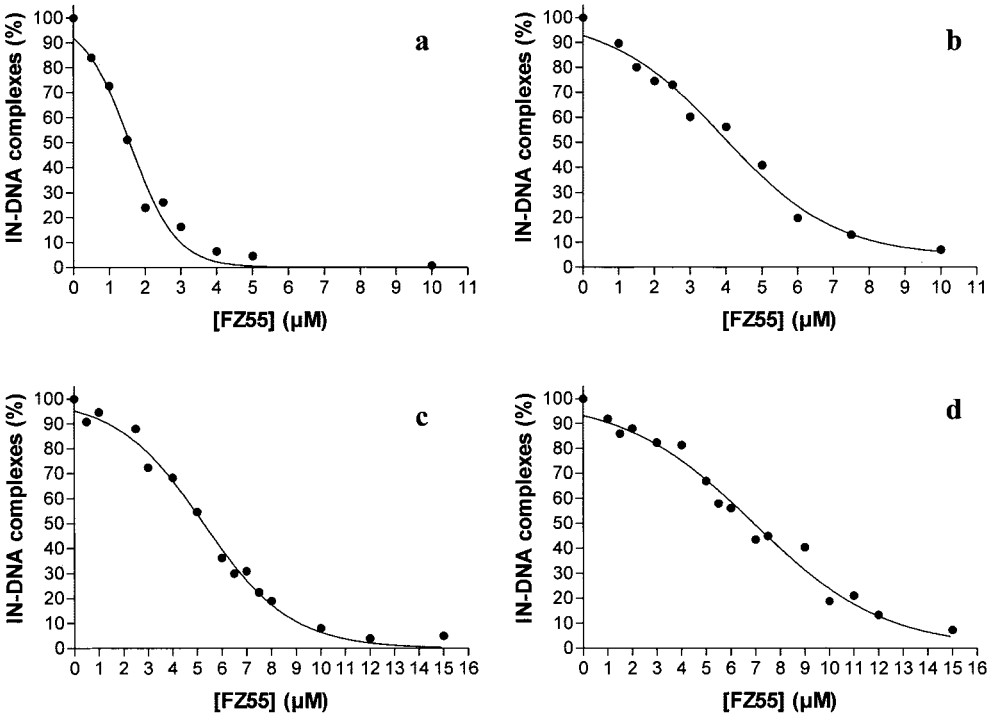

Fig. 6. Percentage of integrase-oligonucleotide complexes as a function of FZ55 and integrase concentrations. Steady-state fluorescence anisotropies were measured at 25°C as described under *Materials and Methods*. a, [IN] = 120 nM; b, [IN] = 240 nM; c, [IN] = 360 nM; d, [IN] = 480 nM. The IC_{50} values together with those obtained at 37°C are reported in Table 4.

in Fig. 7. This finding was confirmed by simulations of inhibition curves using eq. 10 and according to the K_i and K_d values calculated in the previous section. Two examples are shown in Fig. 8, using two different IN concentrations [120 nM (Fig. 6a) and 240 nM (Fig. 6b)]. When n was equal to 1, the shape was hyperbolic and was not consistent with the experimental data. It was thus necessary to increase n to fit the experimental curves. A Hill coefficient of approximately 2.5 was found, which is compatible with the value of 1.9 found in direct binding isotherm experiments. The nonhyperbolic shape of the inhibition curves shown in Fig. 6 can therefore be explained by the positive cooperative binding of IN to DNA.

At higher DNA substrate concentrations (>10 nM), the 3′-processing activity decreased (data not shown). The most plausible explanation for this is that the active multimeric form of IN is not favorable at this high DNA substrate/IN ratio. According to the steady-state fluorescence anisotropy data, it seems that a simple 1:1 model of IN/viral DNA interaction is not sufficient to fit the experimental data of both binding isotherm and inhibition. A cooperative model is more appropriate and gives a Hill coefficient of between 1.9 and 2.5. In a previous study, we found a monomeric form of IN bound to DNA at 25°C and a monomer-dimer equilibrium at 37°C (Deprez et al., 2001). These results were obtained at a low IN/DNA ratio (from 5 to 10). Given the K_d value found here (apparent K_d, ~35 nM), these conditions were not favorable to observe multimeric forms of IN onto DNA. Here, the IN/DNA ratios were much higher at both 25°C and 37°C (from 120 to 480), which could explain the cooperativity of DNA-binding, which is clear from the direct binding of IN to DNA (Table 3) and the displacement of the equilibrium in the presence of SQs (Fig. 8).

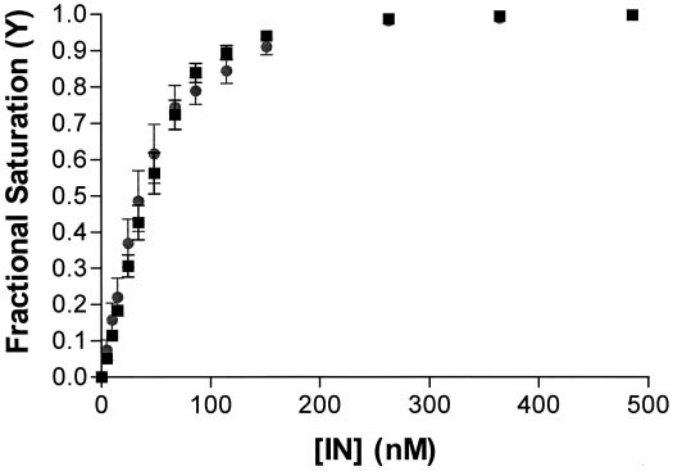

Fig. 7. Binding isotherms for IN-oligonucleotide interactions. The concentration of fluorescein-labeled DNA was 1 nM. Various IN concentrations were preincubated with DNA at 25°C (■) or 37°C (◉) for 20 min to reach equilibrium. Steady-state fluorescence anisotropies were then measured at the same temperatures.

TABLE 3
Parameters for the IN-DNA binding isotherm

	IN_{50} or apparent K_d	Hill Coefficient	Anisotropy Amplitude
25°C	37.5 ± 3.5nM	1.88 ± 0.04	0.183 ± 0.014
37°C	39.2 ± 8 nM	1.81 ± 0.08	0.180 ± 0.006

TABLE 4
IC50 and Ki for FZ55 at different IN concentrations
K_i was calculated from eq. 11. The apparent K_d values at 25° C and 37°C in eq. 11 were obtained from the plot shown in Fig. 7.

	[Integrase]	IC_{50}	K_i	$(IN)^n_H/[(IN)^n_H+(IN_{50})^n_H]$
	nM	*nM*	*nM*	
25°C	120	1575 ± 197	670	0.899
	240	3930 ± 623	687	0.970
	360	5270 ± 227	573	0.986
	480	6930 ± 374	548	0.991
37°C	120	2340 ± 174	1090	0.883
	240	4540 ± 264	844	0.964
	360	6900 ± 411	802	0.982
	480	9810 ± 588	832	0.989

Styrylquinolines Do Not Inhibit the 3′-Processing Activity of Preformed IN-DNA Complexes. Our results show that the inhibition of 3′-processing is probably caused by a competition mechanism between the drug and the DNA substrate. Because IN-DNA complexes display half-lives of a few hours, without turnover of the enzymes during the reaction (Lee et al., 1995; Pemberton et al., 1996), SQs must act on free IN and can only efficiently block IN when preincubated with the enzyme. They should not inhibit 3′-processing performed by preformed IN-DNA complexes. This idea is reinforced by the results of the DNA-binding assays described above. To address this hypothesis, we compared the effect of SQs on the 3′-processing reaction when IN was preincubated with KHD161 before adding the DNA substrate and when IN was allowed to form a complex with its cognate DNA substrate before adding the inhibitor (Fig. 9). First, KHD161 was incubated with 50 nM IN before the addition of

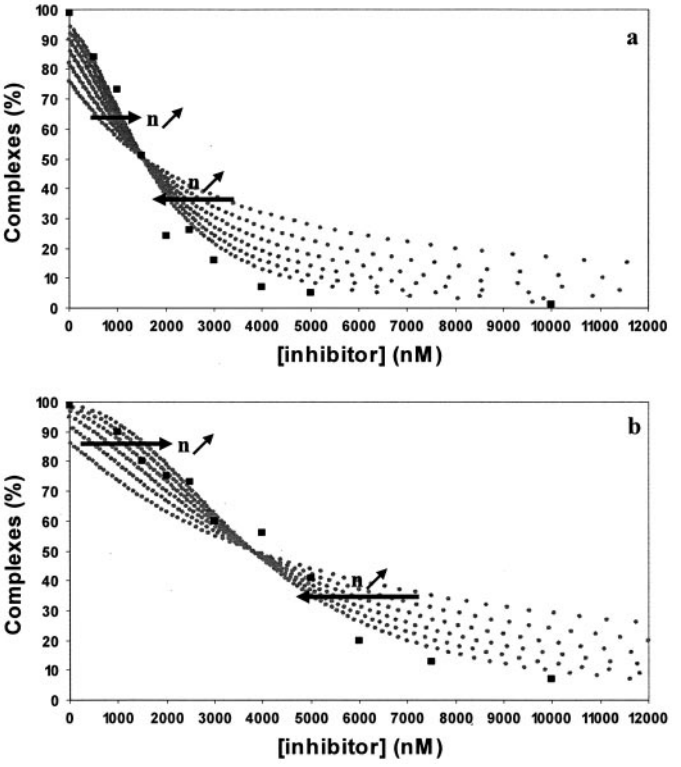

Fig. 8. Simulation of the Hill coefficient effect on the inhibition curves. a, 120 nM IN; b, 240 nM IN. ■, experimental data. ◉, simulations using equation 10. The Hill number (n) increases from 1 to 2.5 (in increments of 0.3), as indicated by the black arrows.

the DNA substrate (Fig. 9, lanes 1–8). Submicromolar inhibition was observed, with an IC_{50} of 0.4 μM. This value was lower than that determined above (1.2 μM) because the concentration of IN was lower (50 nM compared with 120 nM). Second, IN/LTR complexes were preformed for 20 min at 25°C in the presence of Mg^{2+}, because it has been shown previously that the amount of complexes is optimal at this time (Brodin et al., 2002). The drug was then added and the reaction was allowed to proceed at 37°C (Fig. 9, lanes 9–15). In a control experiment, a metal chelator, EDTA, was added immediately after the preincubation period to ensure that no 3′-processing could take place during this step. In the presence of EDTA, only a low level of residual activity was observed (lane 16), demonstrating that the 3′-processing activity observed in the absence of EDTA mainly occurred during the incubation at 37°C. In this condition, the inhibition by the SQ was dramatically decreased, with an IC_{50} of more than 30 μM. Thus, this compound was much less efficient in inhibiting the 3′-processing activity of the preformed IN-DNA substrate complex because of its inability to disrupt the complex.

Styrylquinoline Derivatives Inhibit Strand Transfer Activity of Immobilized IN-DNA Complex. SQs cannot inhibit the 3′-processing of preformed complexes. However, because strand transfer requires the binding of a second DNA molecule to the processed DNA-enzyme complex, our data did not allow us to draw any conclusions about their abilities to act as strand transfer inhibitors. Unlike inhibitors such as DKA derivatives, which specifically impair the strand transfer process, SQ compounds efficiently inhibit the 3′-processing reaction. However, in overall standard in vitro activity assays using oligonucleotides that mimic one LTR extremity, the strand transfer products correspond to the transfer of a processed DNA into a homologous DNA. In the case of SQ, inhibition of the 3′-processing reaction obviously leads to a marked decrease in the amount of strand transfer products. This observation does not necessarily mean that SQs are potent inhibitors of the strand transfer process because the apparent inhibitory effect may simply result from the disappearance of the substrate of the strand transfer reaction. On the other hand, classic strand transfer assays using preprocessed DNAs may only reveal the propensity of drugs to inhibit the binding of IN to its DNA substrate. To test whether SQs can inhibit the strand transfer independently of the 3′-processing reaction, we assayed this activity on a preformed IN-DNA complex. The viral preprocessed DNA substrate (LDS31A/LDS32Bp) was immobilized on the NH2-activated surface of a microtiter plate and the IN-DNA complex was formed by allowing IN to bind to the substrate for 20 min. Free IN was removed, and biotin-labeled double-stranded DNA target was added in the presence of the SQ derivative. A dose-dependent inhibitory effect was observed when SQ was added after the formation of the IN/DNA complex (Fig. 10). The IC_{50} value in this condition was approximately 6 μM. In a control experiment (not shown), KHD161 was added before IN to determine the inhibition of strand transfer caused by the impairment of IN-binding to its substrate DNA. The IC_{50} value was about 1 μM. Although the IC_{50} value obtained for the preformed complex, 6 μM, was higher than that observed when the drug was present before the formation of the complex, this result indicates that SQs also inhibit the strand transfer reaction.

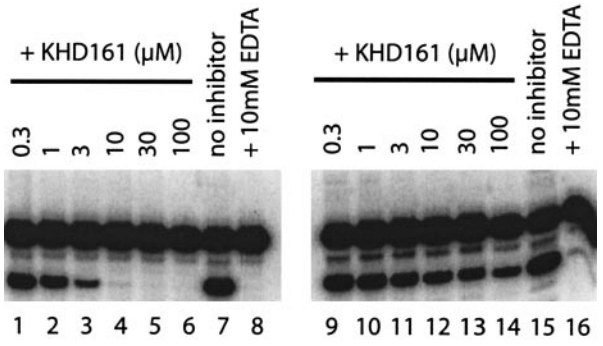

Fig. 9. Comparison of the effects of styrylquinoline on the free IN and preassembled DNA-IN complexes for the 3′-processing reaction. IN was incubated with the U5 blunt substrate for 20 min at room temperature to allow formation of the IN-DNA complex. The 3′-processing reaction was subsequently started by increasing the temperature to 37°C and allowed to proceed for 1 h. A control reaction was quenched by adding EDTA at t = 20 min to determine the reaction yield during the preincubation period. Increasing concentrations of KHD161 were added before (lanes 1–8) or after (lanes 9–16) the formation of IN-DNA complexes. Drug concentrations: lanes 1 and 9, 0.3 μM; lanes 2 and 10, 1 μm; lanes 3 and 11, 3 μm; lanes 4 and 12, 10 μM; lanes 5 and 13, 30 μM; lanes 6 and 14, 100 μM; lanes 7 and 15, no inhibitor; lanes 8 and 16, no inhibitor and 10 mM EDTA.

Discussion

Our experimental data indicate that SQ compounds are pure competitive inhibitors of the 3′-processing reaction. SQs inhibit the formation of the IN-viral DNA complexes with K_i values of 0.4 to 0.9 μM. The fluorescence spectral study of one derivative strongly supports a direct binding of SQ to IN. Two of the three protein domains display a DNA-binding activity

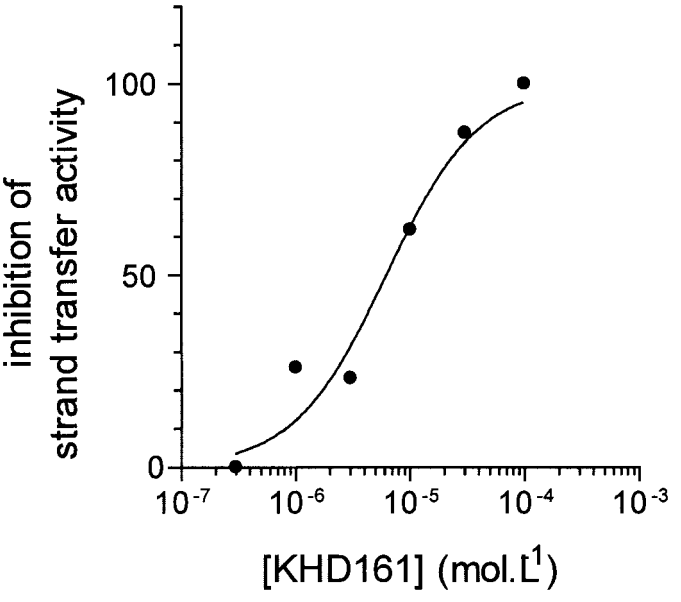

Fig. 10. Inhibition of strand transfer reaction on immobilized IN-U5–2 complex by KHD161. HIV-1 IN (100 nM) was incubated with preprocessed U5 substrate covalently immobilized on a microtiter plate for 20 min at room temperature. Free IN was subsequently removed. The reaction was started by increasing the temperature to 37°C and allowed to proceed for 1 h. The reaction mixture included 130 nM of biotin-labeled double-stranded DNA target and increasing concentrations of KHD161 compound. The reaction was stopped by adding EDTA. Strand transfer products were quantified by measuring phosphatase activity as indicated under *Materials and Methods*. Inhibition is indicated as a percentage of the control activity.

and are therefore potential targets: the catalytic core, which contains the catalytic triad, and the C-terminal domain, which stabilizes the DNA-protein interaction. Previous inhibition experiments of the core domain-mediated disintegration reaction by SQs strongly suggested that this domain was the target (Zouhiri et al., 2000). The docking data with the HIV-1 catalytic core confirm this hypothesis. These data indicate the existence of stable interactions between SQ and the core domain near the DDE triad (cluster 1) and other residues known to make contacts with DNA. Moreover, these interactions remained stable over a 2-ns MD.

SQs were efficient when they were added before the formation of IN-DNA complexes, suggesting that once bound to the target, IN, they prevent DNA binding as suggested by computational docking. This mechanism was confirmed by fluorescence anisotropy assays. The addition of SQs prevented the formation of IN-DNA complexes in a manner that is compatible with the decrease in the 3′-processing activity. Therefore, SQs do not act in the subsequent catalysis step. Furthermore, SQs were unable to disrupt preformed complexes and did not inhibit the 3′-processing of the preformed IN-viral DNA complex. This is in agreement with other data showing that IN-DNA complexes are very stable ($t_{1/2}$ = 1 h) and characterized by a very slow turnover (k_{cat} = 0.04–0.06 min^{-1}) (Lee et al., 1995; Pemberton et al., 1996). Thus, the very slow dissociation rate of the IN-DNA complex does not allow competition with SQ to take place within the duration of the experiments described here.

The in vitro inhibition activity of styrylquinoline is mainly related to the simultaneous presence of a carboxyl group at C-7 (Zouhiri et al., 2000) and a hydroxyl group at C-8 in the quinoline subunit (this study; see FZ117). At experimental pH, close to neutrality, KHD161 and FZ55 probably have a net charge of −1 (reinforcing the hypothesis that DNA is not a ligand for these drugs) and are most likely stabilized in the active site through interactions between the *o*-hydroxy acid group (7-COO^-/8-OH) and the Mg^{2+} cofactor. The enol form is more favorable in aqueous medium, but the keto form has more favorable interaction energy in the active site context. Such interactions are compatible with an enthalpy-driven association of the drug with the active site as found using steady-state fluorescence anisotropy assay. In contrast, IN-DNA interactions seem to be driven primarily by entropy, probably because of a large solvent contribution (the release of water from large protein-DNA interfaces is entropically favorable).

Using assays that make it possible to test independently the inhibition effect on the strand transfer process performed by a preformed complex between IN and the preprocessed viral DNA substrate, we found that SQs may significantly inhibit the subsequent integration reaction into a heterologous target DNA. The corresponding IC_{50} value was higher than that measured for 3′-processing (6 versus 1 μM, respectively). Two models can explain this result: 1) SQs may target and actively disrupt the preformed complex. This hypothesis is unlikely because we established that SQs do not efficiently inhibit the 3′-processing of the preformed IN-viral DNA complex. This means that once the IN-viral DNA or the IN-preprocessed viral DNA complex is established, it cannot be disrupted by competitive drugs. 2) SQs may bind to a second site within the active site in a manner that competitively inhibits the binding of the second substrate, the target DNA. This secondary binding site that prevents the target DNA from binding could be close to the first one that prevents the viral DNA from binding, yet distinct in the active site. In this binding mode, SQs would act similarly to DKA compounds (Espeseth et al., 2000). However, one major difference between SQ and DKA compounds is that SQs have a lower affinity for the target DNA binding site; the IC_{50} values for strand transfer are significantly higher than the values found for 3′-processing. The situation is very different for the DKAs because they do not bind efficiently to the active site of the DNA-free IN (Espeseth et al., 2000). Based on our results, we cannot determine whether SQs also bind to the second site in the context of the DNA-free IN or only when the first DNA substrate is already bound, as is observed with DKAs.

From computational simulations, it seems that cluster 1 is very likely to be the primary binding site for SQs. This cluster, which corresponds to one of the two proposed DNA-binding sites (Perryman and McCammon, 2002), contains the catalytic triad and several key residues for DNA binding. This cluster is characterized by a positive electrostatic potential created by residues Lys156, Lys159, and His67. The average interaction energy is better in cluster 1 than in other clusters. Moreover, unlike clusters 2 and 3, the interaction energy is strongly affected by the proximity of Mg^{2+} in this cluster in accordance with experiments. In fact, IN has much less effect on the fluorescence properties of FZ55 in the absence of Mg^{2+} or in the presence of EDTA. Nevertheless, clusters 2 and 3 may be candidates for the secondary binding site. It is not clear which one is actually the target, but cluster 3 contains two key residues for DNA-binding (Mazumder et al., 1996; Esposito and Craigie, 1998) and corresponds to one DNA binding site proposed by Perryman and McCammon (2002). Nevertheless, our docking data were obtained with the DNA-free protein, and we cannot rule out the idea that the secondary SQ-bindinq site is created by the binding of DNA in a manner similar to that described previously for DKAs. In that case, the role of a second Mg^{2+} in the active site could be crucial for the stabilization of the SQ in the second binding site.

A recent study (Marchand et al., 2002) suggests that two different binding sites for DKAs may coexist in the active site and the donor and the acceptor sites. Accordingly, a DKA compound, such as L-708,906, that preferentially inhibits the strand transfer reaction, binds within the acceptor site. Bifunctional DKAs and a DKA-related compound, 5-CITEP, are less selective and seem to bind both donor and acceptor sites. SQs behaves similarly, and the existence of two binding modes may be extended to many compounds having both aromatic and carboxylate groups. Therefore, it seems that all these compounds share a common competitive mechanism of action, with a more pronounced effect against either donor or acceptor DNA-binding depending on their relative affinities for the corresponding binding sites. L-708,906 displays extreme behavior; it has a very low and a very high affinity for the donor and acceptor sites, respectively. The bifunctional DKA and 5-CITEP bind to both sites but have a higher affinity for the acceptor site because they are better able to inhibit the strand transfer than the 3′-processing. Finally, SQs can efficiently inhibit 3′-processing and exhibit significant proper activity on the strand transfer reaction starting from a preassembled IN-preprocessed viral DNA complex. According to the IC_{50} values obtained for the two catalytic

steps, SQs probably have a greater affinity (5- to 10-fold) for the donor site than for the acceptor site, in contrast to that observed for Merck or Shionogi inhibitor.

It is widely believed that the stable IN-DNA interaction within the preintegration complex precludes inhibitors acting as competitor of donor DNA from being effective in the cellular context. If this is correct, compounds that inhibit 3′-processing in vitro in a competitive manner should be unable to block viral replication. However, although most 3′-processing inhibitors actually lack antiviral effect, this is not the case for SQs (Zouhiri et al., 2000) and other 3′-processing inhibitors such as pyranodipyrimidine compounds (Pannecouque et al., 2002), which show a moderate activity ex vivo. Several hypothesizes may account for this apparent discrepancy. First, in light of our data, the ex vivo activity of SQs could still be related to their ability to inhibit the strand transfer reaction. Because SQ derivatives are less efficient against strand transfer than 3′-processing in vitro, this hypothesis could explain the micromolar antiviral activity detected ex vivo. Recently, another series of IN inhibitors that is not specific for strand transfer in vitro was shown to effectively prevent HIV replication by inhibiting integration (Pannecouque et al., 2002). Second, we cannot rule out the possibility that the active site of IN is accessible, at least transiently, during the early steps of replication. If this is the case, the 3′-processing reaction could be affected by SQs. The early targeting of IN might also affect revers transcriptase, because functional interactions between both proteins have been described. In fact, the KRK (186–188) motif of IN has been described to play a major role in the efficiency of reverse transcription (Tsurutani et al., 2000) and two residues of this motif, Lys186 and Lys188, were present in cluster 2 of our docking study. Finally, the IN-inhibitor interaction may alter the karyophilic properties of the enzyme, which are required for the nuclear translocation of the preintegration complex. It is noteworthy that a single structural protein domain may be simultaneously involved in both DNA-binding and nuclear localization (Nissen et al., 2000). Studies on the ex vivo mechanism(s) of inhibition of HIV replication by SQs are in progress.

Acknowledgments

We thank Françoise Simon for technical assistance. M.K. and M.L.B. are grateful for access to the O2000 multiprocessor of Pôle Parallélisme IdF Sud.

References

Brodin P, Pinskaya M, Buckle M, Parsch U, Romanova E, Engels J, Gottikh M, and Mouscadet JF (2002) Disruption of HIV-1 integrase-DNA complexes by short 6-oxocytosine-containing oligonucleotides. *Biochemistry* **41:**1529–1538.

Burdujan R (2002) *Dynamique reactionnelle d'inhibiteurs de l'integrase du VIH-1: de la solution au milieu cellulaire*. Thesis, University Paris XI, Orsay, France.

Cheng Y and Prusoff WH (1973) Relationship between the inhibition constant (K1) and the concentration of inhibitor which causes 50 per cent inhibition (I50) of an enzymatic reaction. *Biochem Pharmacol* **22:**3099–3108.

Chow SA, Vincent KA, Ellison V, and Brown PO (1992) Reversal of integration and DNA splicing mediated by integrase of human immunodeficiency virus. *Science (Wash DC)* **255:**723–726.

Craigie R (2001) HIV integrase, a brief overview from chemistry to therapeutics. *J Biol Chem* **276:**23213–23216.

Deprez E, Tauc P, Leh H, Mouscadet JF, Auclair C, and Brochon JC (2000) Oligomeric states of the HIV-1 integrase as measured by time-resolved fluorescence anisotropy. *Biochemistry* **39:**9275–9284.

Deprez E, Tauc P, Leh H, Mouscadet JF, Auclair C, Hawkins ME, and Brochon JC (2001) DNA binding induces dissociation of the multimeric form of HIV-1 integrase: a time-resolved fluorescence anisotropy study. *Proc Natl Acad Sci USA* **98:**10090–10095.

Drake RR, Neamati N, Hong H, Pilon AA, Sunthankar P, Hume SD, Milne GW, and Pommier Y (1998) Identification of a nucleotide binding site in HIV-1 integrase. *Proc Natl Acad Sci USA* **95:**4170–4175.

Espeseth AS, Felock P, Wolfe A, Witmer M, Grobler J, Anthony N, Egbertson M, Melamed JY, Young S, Hamill T, et al. (2000) HIV-1 integrase inhibitors that compete with the target DNA substrate define a unique strand transfer conformation for integrase. *Proc Natl Acad Sci USA* **97:**11244–11249.

Esposito D and Craigie R (1998) Sequence specificity of viral end DNA binding by HIV-1 integrase reveals critical regions for protein-DNA interaction. *EMBO (Eur Mol Biol Organ) J* **17:**5832–5843.

Ewald P (1921) Die Berechnung Optischer und Elektrostatischer Gitterpotentiale. *Ann Phys* **64:**253–287.

Goldgur Y, Craigie R, Cohen GH, Fujiwara T, Yoshinaga T, Fujishita T, Sugimoto H, Endo T, Murai H, and Davies DR (1999) Structure of the HIV-1 integrase catalytic domain complexed with an inhibitor: a platform for antiviral drug design. *Proc Natl Acad Sci USA* **96:**13040–13043.

Goldgur Y, Dyda F, Hickman AB, Jenkins TM, Craigie R, and Davies DR (1998) Three new structures of the core domain of HIV-1 integrase: an active site that binds magnesium. *Proc Natl Acad Sci USA* **95:**9150–9154.

Harper AL, Skinner LM, Sudol M, and Katzman M (2001) Use of patient-derived human immunodeficiency virus type 1 integrases to identify a protein residue that affects target site selection. *J Virol* **75:**7756–7762.

Hazuda DJ, Felock P, Witmer M, Wolfe A, Stillmock K, Grobler JA, Espeseth A, Gabryelski L, Schleif W, Blau C, et al. (2000) Inhibitors of strand transfer that prevent integration and inhibit HIV-1 replication in cells. *Science (Wash DC)* **287:**646–650.

Hazuda DJ, Hastings JC, Wolfe AL, and Emini EA (1994) A novel assay for the DNA strand-transfer reaction of HIV-1 integrase. *Nucleic Acids Res* **22:**1121–1122.

Jenkins TM, Esposito D, Engelman A, and Craigie R (1997) Critical contacts between HIV-1 integrase and viral DNA identified by structure-based analysis and photocrosslinking. *EMBO (Eur Mol Biol Organ) J* **16:**6849–6859.

Jing N, Marchand C, Liu J, Mitra R, Hogan ME, and Pommier Y (2000) Mechanism of inhibition of HIV-1 integrase by g-tetrad-forming oligonucleotides in vitro. *J Biol Chem* **275:**21460–21467.

Laboulais C, Deprez E, Leh H, Mouscadet JF, Brochon JC, and Le Bret M (2001) HIV-1 integrase catalytic core: molecular dynamics and simulated fluorescence decays. *Biophys J* **81:**473–489.

Laboulais C, Ouali M, Le Bret M, and Gabarro-Arpa J (2002) Hamming distance geometry of a protein conformational space: application to the clustering of a 4-ns molecular dynamics trajectory of the HIV-1 integrase catalytic core. *Proteins* **47:**169–179.

Lavery R, Sklenar H, Zakrzewska K, and Pullman B (1986) The flexibility of the nucleic acids: (II). The calculation of internal energy and applications to mononucleotide repeat DNA. *J Biomol Struct Dyn* **3:**989–1014.

Lee SP, Kim HG, Censullo ML, and Han MK (1995) Characterization of Mg^{2+}-dependent 3′-processing activity for human immunodeficiency virus type 1 integrase in vitro: real-time kinetic studies using fluorescence resonance energy transfer. *Biochemistry* **34:**10205–10214.

Leh H, Brodin P, Bischerour J, Deprez E, Tauc P, Brochon JC, LeCam E, Coulaud D, Auclair C, and Mouscadet JF (2000) Determinants of Mg^{2+}-dependent activities of recombinant human immunodeficiency virus type 1 integrase. *Biochemistry* **39:**9285–9294.

Linden J (1982) Calculating the dissociation constant of an unlabeled compound from the concentration required to displace radiolabel binding by 50%. *J Cyclic Nucleotide Res* **8:**163–172.

Maignan S, Guilloteau JP, Zhou-Liu Q, Clement-Mella C, and Mikol V (1998) Crystal structures of the catalytic domain of HIV-1 integrase free and complexed with its metal cofactor: high level of similarity of the active site with other viral integrases. *J Mol Biol* **282:**359–368.

Marchand C, Zhang X, Pais GC, Cowansage K, Neamati N, Burke TR Jr, and Pommier Y (2002) Structural determinants for HIV-1 integrase inhibition by β-diketo acids. *J Biol Chem* **277:**12596–12603.

Mazumder A, Neamati N, Pilon AA, Sunder S, and Pommier Y (1996) Chemical trapping of ternary complexes of human immunodeficiency virus type 1 integrase, divalent metal and DNA substrates containing an abasic site. Implications for the role of lysine 136 in DNA binding. *J Biol Chem* **271:**27330–27338.

Mekouar K, Mouscadet JF, Desmaele D, Subra F, Leh H, Savoure D, Auclair C, and d'Angelo J (1998) Styrylquinoline derivatives: a new class of potent HIV-1 integrase inhibitors that block HIV-1 replication in CEM cells. *J Med Chem* **41:**2846–2857.

Ni H, Sotriffer CA, and McCammon JA (2001) Ordered water and ligand mobility in the HIV-1 integrase-5CITEP complex: a molecular dynamics study. *J Med Chem* **44:**3043–3047.

Nissen P, Kjeldgaard M, and Nyborg J (2000) Macromolecular mimicry. *EMBO (Eur Mol Biol Organ) J* **19:**489–495.

Ouali M, Laboulais C, Leh H, Gill D, Desmaele D, Mekouar K, Zouhiri F, d'Angelo J, Auclair C, Mouscadet JF, et al. (2000) Modeling of the inhibition of retroviral integrases by styrylquinoline derivatives. *J Med Chem* **43:**1949–1957.

Pannecouque C, Pluymers W, Van Maele B, Tetz V, Cherepanov P, De Clercq E, Witvrouw M, and Debyser Z (2002) New class of HIV integrase inhibitors that block viral replication in cell culture. *Curr Biol* **12:**1169–1177.

Pemberton IK, Buckle M, and Buc H (1996) The metal ion-induced cooperative binding of HIV-1 integrase to DNA exhibits a marked preference for Mn(II) rather than Mg(II). *J Biol Chem* **271:**1498–1506.

Perryman AL and McCammon JA (2002) AutoDocking dinucleotides to the HIV-1 integrase core domain: exploring possible binding sites for viral and genomic DNA. *J Med Chem* **45:**5624–5627.

Polanski J, Zouhiri F, Jeanson L, Desmaele D, d'Angelo J, Mouscadet JF, Gieleciak R, Gateiger J, and Le Bret M (2002) Use of the Kohonen neural network for rapid screening of ex vivo anti-HIV activity of styrylquinolines. *J Med Chem* **45:**4647–4654.

Pommier Y, Marchand C, and Neamati N (2000) Retroviral integrase inhibitors year 2000: update and perspectives. *Antiviral Res* **47:**139–148.
Ryckaert JP, Cicotti G, and Berendsen H (1977) Numerical integration of the cartesian equations of motion of a system with constraints: molecular dynamics of n-alkanes. *J Comp Phys* **23:**327–341.
Tsurutani N, Kubo M, Maeda Y, Ohashi T, Yamamoto N, Kannagi M, and Masuda T (2000) Identification of critical amino acid residues in human immunodeficiency virus type 1 IN required for efficient proviral DNA formation at steps prior to integration in dividing and nondividing cells. *J Virol* **74:**4795–4806.
Zhuang L, Wai JS, Embrey MW, Fisher TE, Egbertson MS, Payne LS, Guare JP Jr, Vacca JP, Hazuda DJ, Felock PJ, et al. (2003) Design and synthesis of 8-hydroxy-[1, 6]naphthyridines as novel inhibitors of HIV-1 integrase in vitro and in infected cells. *J Med Chem* **46:**453–456.
Zouhiri F, Mouscadet JF, Mekouar K, Desmaele D, Savoure D, Leh H, Subra F, Le Bret M, Auclair C, and d'Angelo J (2000) Structure-activity relationships and binding mode of styrylquinolines as potent inhibitors of HIV-1 integrase and replication of HIV-1 in cell culture. *J Med Chem* **43:**1533–1540.

Address correspondence to: Jean-François Mouscadet, UMR CNRS-8113, Laboratoire de Biotechnologies et Pharmacologie Génétique Appliquée (L.B.P.A.), Ecole Normale Supérieure de Cachan, 61 avenue du Président Wilson, 94235 Cachan Cedex, France. E-mail: mouscadet@lbpa.ens-cachan.fr